

## Scaling of asymmetric magnetic reconnection: Kinetic particle-in-cell simulations

K. Malakit,<sup>1</sup> M. A. Shay,<sup>1</sup> P. A. Cassak,<sup>2</sup> and C. Bard<sup>1</sup>

Received 12 March 2010; revised 8 June 2010; accepted 14 July 2010; published 12 October 2010.

[1] Recently, Cassak and Shay (2007) applied a generalized Sweet-Parker analysis to derive scaling laws for gross properties of asymmetric magnetic reconnection, including the reconnection rate, outflow speed, and outflow density. This study presents the first comprehensive test of this scaling theory using fully electromagnetic particle-in-cell simulations of antiparallel asymmetric magnetic reconnection. By varying the upstream densities and magnetic fields, we find that the reconnection rates, outflow speeds, and outflow densities are consistent with the general scaling theory. This implies that kinetic electron and proton physics beyond the Hall term does not fundamentally alter the gross properties of the asymmetric diffusion region as understood in Cassak and Shay (2007). In addition, the results confirm the validity of the assumption of mixing of particles on recently reconnected flux tubes, which is of key importance for accurately predicting the location of the flow stagnation point in the diffusion region.

**Citation:** Malakit, K., M. A. Shay, P. A. Cassak, and C. Bard (2010), Scaling of asymmetric magnetic reconnection: Kinetic particle-in-cell simulations, *J. Geophys. Res.*, 115, A10223, doi:10.1029/2010JA015452.

### 1. Introduction

[2] Conventional studies of magnetic reconnection have mainly focused on symmetric reconnection where the magnetic field and particle density are the same on both sides upstream of the diffusion region [e.g., *Birn et al.*, 2001, and references therein]. However, in many physical situations the magnetic field and density in these two upstream regions can vary substantially. Dayside reconnection, where magnetosheath plasma (magnetic field  $\approx 10$ – $20$  nT, density  $\approx 20$ – $30$  cm<sup>-3</sup>) reconnects with magnetospheric plasma (magnetic field  $\approx 50$ – $60$  nT, density  $\approx 0.3$ – $0.5$  cm<sup>-3</sup>), is a good example of this so-called “asymmetric reconnection” [*Phan and Paschmann*, 1996; *Mozer et al.*, 2008a, and references therein]. As another example, asymmetric reconnection has been observed in the magnetotail [*Øieroset et al.*, 2004].

[3] To understand asymmetric reconnection, *Cassak and Shay* [2007] introduced a model of the asymmetric diffusion region on which they performed a Sweet-Parker-type scaling analysis. They then obtained scaling relations predicting asymmetric reconnection properties including reconnection rate, outflow speed, outflow density, x line position, and stagnation point position as functions of upstream magnetic fields and particle densities. This general theory was consistent with a previous scaling analysis for asymmetric

density [*Borovsky and Hesse*, 2007], and the reconnection rate and outflow speed predictions have been verified thoroughly with fluid simulations for both collisional [*Cassak and Shay*, 2007; *Borovsky et al.*, 2008; *Servidio et al.*, 2009] and collisionless reconnection [*Cassak and Shay*, 2008]. A systematic study of the scaling results have not been carried out using more realistic particle-in-cell codes. However, various predictions have been borne out in PIC simulations [*Mozer et al.*, 2008b; *Pritchett*, 2008; *Tanaka et al.*, 2008]. The reconnection rate scaling was used to determine a physics-based solar wind/magnetosphere coupling model which showed similar or better correlations with various empirical geomagnetic indices than previous coupling models [*Borovsky*, 2008]. We emphasize that the focus of this paper is on the scaling of the diffusion region during asymmetric reconnection. See *Cassak and Shay* [2007] for references on other aspects of asymmetric reconnection.

[4] One important aspect of the theory, however, has not been borne out by simulations. A basic assumption of the scaling study was that in the asymmetric density case, the plasmas with disparate densities in two recently reconnected flux tubes will quickly mix while at the same time conserving the total flux tube volume [*Cassak and Shay*, 2007], which allows the determination of the outflow density and the location of the stagnation point. This assumption has been called into question by MHD and two-fluid simulations results [*Birn et al.*, 2008; *Cassak and Shay*, 2009], where parallel pressure balance along flux tubes prevents mixing, leading to stagnation point locations that do not match predictions. Modification of the scaling theory to remove the mixing assumption, while predicting the fluid stagnation point, leads to erroneous predictions of the X line location [*Cassak and Shay*, 2009].

<sup>1</sup>Department of Physics and Astronomy, University of Delaware, Newark, Delaware, USA.

<sup>2</sup>Department of Physics, West Virginia University, Morgantown, West Virginia, USA.

[5] The failure of the stagnation point predictions in fluid simulations highlights the need for a systematic simulation study of asymmetric reconnection which includes kinetic effects such as parallel thermal diffusion [Nakamura and Scholer, 2000]. Such a study can directly test the downstream mixing assumption for collisionless systems such as the Earth's magnetosphere. In addition, there is the outstanding question of whether the inclusion of kinetic physics beyond the Hall term fundamentally alters the diffusion region structure and require a significant revision of the scaling theory.

[6] In this study, we perform a systematic set of electromagnetic kinetic particle-in-cell (PIC) simulations of collisionless asymmetric reconnection and compare various gross diffusion region properties with analytical scaling predictions. We find that the simulation results for reconnection rates and ion outflow speeds agree well with the predictions of scaling theory [Cassak and Shay, 2007], which suggests that the kinetic physics beyond Hall term does not fundamentally alter ion scale properties of the diffusion region. Moreover, the density just downstream of the diffusion region is in good agreement with the prediction, implying that volume conserving particle mixing along newly reconnected flux tubes is a good approximation.

## 2. Theory

[7] In order to understand the properties of asymmetric reconnection, Cassak and Shay [2007] generalized the Sweet-Parker-type analysis to a case with asymmetric upstream conditions. In this analysis, the steady state diffusion region is assumed to be roughly a rectangular region, outside of which single-fluid MHD is assumed to be applicable. Using conservation of mass and energy across the boundaries of the diffusion region and the sub boxes delineated by the X line and stagnation point, they arrived at scaling relations of asymmetric reconnection as functions of the upstream magnetic fields and densities. The results are independent of the process breaking the frozen-in constraint. The resulting scaling laws, therefore, are applicable to both collisional reconnection with a finite resistivity and collisionless reconnection, where the frozen-in condition is broken by kinetic effects.

[8] Two general properties of reconnection, namely, the reconnection electric field  $E$  and the outflow speed  $v_{out}$  are predicted to scale as,

$$E \sim \left( \frac{2B_1B_2}{B_1+B_2} \right) \left( \frac{v_{out}}{c} \right) \left( \frac{\delta}{L} \right) \quad (1)$$

$$v_{out}^2 \sim \frac{B_1B_2}{4\pi m n_{out}}, \quad (2)$$

where  $B$  is the magnetic field,  $n$  is the number density,  $c$  is the speed of light,  $m$  is the particle mass,  $\delta$  is the half width of the dissipation region, and  $L$  is the half-length of the dissipation region. The subscripts "1" and "2" are used to denote the two upstream regions. The outflow number density is  $n_{out}$ , which can be estimated by assuming that the two densities within a recently reconnected flux tube com-

pletely mix while maintaining the original flux tube volume [see Cassak and Shay, 2007, Figure 2]:

$$n_{out} \sim \frac{n_1B_2 + n_2B_1}{B_1 + B_2}. \quad (3)$$

Equations (2) and (3) apply equally well at the ion and electron layers, but we focus on the ion outflow speed and density for the present study.

[9] We emphasize that there are uncertainties in applying these simplistic scaling laws to simulation studies. One clear source of uncertainty is that magnetic fields, densities, and velocities can vary at the edges of the diffusion region, while the theory assumes they are relatively uniform. In addition, the finite Larmor radius of particles in kinetic PIC simulations give them meandering orbits in the diffusion region. A single particle may therefore spend part of its orbit in the diffusion region, and part of its orbit outside, leading to only partial acceleration of the particle by diffusion region electric fields. Because of these uncertainties, the Sweet-Parker-type analysis can only be expected to hold up to a constant of order unity, and expressions are denoted with a  $\sim$  instead of a  $\approx$ .

## 3. Simulations and Results

[10] We use the parallel particle-in-cell code P3D [Zeiler et al., 2002] to perform simulations in 2 1/2 dimensions of collisionless anti-parallel asymmetric reconnection. In the simulations, magnetic field strengths are normalized to an arbitrary value  $B_0$ . Particle number densities are normalized to an arbitrary value  $n_0$ . Lengths are normalized to the ion inertial length  $d_{i0} = c/\omega_{pi}$  at the reference density. Time is normalized to the ion cyclotron time  $\Omega_{ci0}^{-1} = (eB_0/m_i c)^{-1}$ . Speeds are normalized to the Alfvén speed  $c_{A0} = B_0/(4\pi m_i n_0)^{1/2}$ . The speed of light,  $c$ , is set to be  $15c_{A0}$ . Electric fields and temperatures are normalized to  $E_0 = c_{A0}B_0/c$  and  $T_0 = m_i c_{A0}^2$ , respectively. The electron to ion mass ratio is  $m_e/m_i = 1/25$ .

[11] The position and velocity of each particle are governed by the relativistic form of Newton's second law of motion with the Lorentz force being the only force. Effects due to collisions are not included. In normalized form, the equations of motion for a particle ( $\alpha = i$  for ions and  $e$  for electrons) are:

$$\frac{d\mathbf{x}_\alpha}{dt} = \mathbf{v}_\alpha \quad (4)$$

$$\frac{d}{dt}(\gamma_\alpha \mathbf{v}_\alpha) = \frac{q_\alpha}{e} \frac{m_i}{m_\alpha} \cdot [\mathbf{E} + (\mathbf{v}_\alpha \times \mathbf{B})] \quad (5)$$

where  $\mathbf{x}_\alpha$  is the position of the particle,  $\mathbf{v}_\alpha$  is the velocity of the particle, and  $\gamma_\alpha$  is the Lorentz factor corresponding to the velocity of the particle. The proton charge  $q_i = +e$  and electron charge  $q_e = -e$ . The magnetic and electric fields are governed by Faraday's law and Ampere's law, respectively:

$$\frac{\partial \mathbf{B}}{\partial t} = -\nabla \times \mathbf{E} \quad (6)$$

$$\frac{\partial \mathbf{E}}{\partial t} = c^2[(\nabla \times \mathbf{B}) - \mathbf{J}], \quad (7)$$

**Table 1.** Simulation Information<sup>a</sup>

Run	$B_1$	$B_2$	$n_1$	$n_2$	$T_{i1}$	$T_{i2}$	$T_{e1}$	$T_{e2}$	$\Delta x$	$\Delta t$	$ppg$	$E_z$	$v_{i,out}$	$n_{i,out}$
S1	1.0	1.0	1.0	1.0	1.33	1.33	0.67	0.67	0.10	0.01	200	0.045	0.50	1.15
S2	2.0	2.0	1.0	1.0	1.33	1.33	0.67	0.67	0.05	0.01	50	0.25	1.10	1.20
B1	1.0	1.5	1.0	1.0	1.33	0.92	0.67	0.46	0.05	0.005	50	0.06	0.70	1.125
B2	1.0	2.0	1.0	1.0	1.33	0.33	0.67	0.17	0.05	0.01	50	0.125	0.85	1.15
N1	1.0	1.0	1.0	0.5	1.33	2.67	0.67	1.33	0.05	0.005	50	0.06	0.45	0.80
N2a	1.0	1.0	1.0	0.1	1.33	13.33	0.67	6.67	0.05	0.01	200	0.07	0.80	0.55
N2b	1.0	1.0	1.0	0.1	1.33	13.33	0.67	6.67	0.05	0.01	50	0.075	0.85	0.55
N3	2.0	2.0	1.0	0.1	1.33	13.33	0.67	6.67	0.05	0.01	100	0.35	2.00	0.55
BN1	1.0	2.0	1.0	0.25	1.33	1.33	0.67	0.67	0.05	0.01	50	0.12	1.05	0.825
BN2a	1.0	2.0	1.0	0.1	1.33	3.33	0.67	1.67	0.05	0.01	200	0.125	1.20	0.65
BN2b	1.0	2.0	1.0	0.1	1.33	3.33	0.67	1.67	0.05	0.01	50	0.13	1.05	0.73
BN3	1.5	1.0	1.0	0.2	1.33	8.75	0.67	4.38	0.05	0.01	50	0.13	0.80	0.60
BN4	1.5	1.0	1.0	0.1	1.33	17.5	0.67	8.75	0.05	0.01	50	0.125	1.00	0.45

<sup>a</sup>The data from the column of Run through the column of  $ppg$  are user defined. The last three columns come from the analysis. Run column: S, symmetric; B, asymmetric upstream magnetic field; N, asymmetric upstream density; BN, asymmetric upstream magnetic field and density; a and b denote runs with high  $ppg$  and low  $ppg$ , respectively.

where  $\mathbf{J} = n_i \mathbf{u}_i - n_e \mathbf{u}_e$  is the current density, with  $\mathbf{u}_i$  and  $\mathbf{u}_e$  the ion and electron bulk flow velocities. Bulk flows and fluid densities at each grid point are determined by summing the linearly weighted properties of the particles adjacent to the grid point [Birdsall and Langdon, 1985, p. 308–309]. Charge conservation in a fluid sense is maintained by solving Poisson's equation with a multigrid solver and correcting the electric field.

[12] The simulations are performed in a periodic-boundary domain of size  $L_x \times L_y$ , with  $L_x = 204.8$  and  $L_y = 102.4$  and a grid scale  $\Delta x$  of either 0.05 or 0.1, depending upon what is needed to adequately resolve the debye length and other physical length scales. The time step  $\Delta t$  of the simulations is either 0.005 or 0.01, which is chosen such that  $\Delta t$  is smaller than the electron plasma oscillation times and electron cyclotron times based on densities and magnetic fields in both inflow regions. If necessary,  $\Delta t$  is further reduced to minimize any signs of numerical error. The normalization density  $n_0$  is represented by a specific number of particles per grid cell, or  $ppg$ . The values of  $ppg$  as well as the grid scale and time step for the presented runs are shown in Table 1. The initial conditions are a double current sheet, in which the magnetic field has only an  $x$  component and whose spatial dependence is given by:

$$B_x(y) = \left( \frac{B_2 + B_1}{2} \right) \left[ \tanh\left(\frac{y - 0.25L_y}{w_0}\right) - \tanh\left(\frac{y - 0.75L_y}{w_0}\right) + \tanh\left(\frac{y - 1.25L_y}{w_0}\right) - \tanh\left(\frac{y + 0.25L_y}{w_0}\right) + 1 \right] + \left( \frac{B_2 - B_1}{2} \right), \quad (8)$$

where  $B_1$  and  $B_2$  are the asymptotic magnetic field strength on the “1” and “2” upstream sides, and  $w_0$  is the initial width of the sheet, which is set to be 2 for all runs. The total temperature is initially set to vary as a function of  $y$  in a similar manner as the magnetic field:

$$T(y) = \left( \frac{T_2 + T_1}{2} \right) \left[ \tanh\left(\frac{y - 0.25L_y}{w_0}\right) - \tanh\left(\frac{y - 0.75L_y}{w_0}\right) + \tanh\left(\frac{y - 1.25L_y}{w_0}\right) - \tanh\left(\frac{y + 0.25L_y}{w_0}\right) + 1 \right] + \left( \frac{T_2 - T_1}{2} \right), \quad (9)$$

where  $T_1$  and  $T_2$  are the asymptotic total temperatures. The initial ratio of ion temperature and electron temperature is set to be constant throughout the simulation box with  $T_i/T_e = 2.0$ . Once the magnetic field  $B_x(y)$  and the temperature  $T(y)$  are specified, the particles are loaded with Maxwellian velocity distribution, with random  $x$  position distribution, and with  $y$  position distribution such that the particle number density  $n(y)$  makes the total pressure constant:

$$\frac{B_x^2(y)}{2} + n(y)T(y) = \frac{B_1^2}{2} + n_1 T_1 = \frac{B_2^2}{2} + n_2 T_2, \quad (10)$$

where  $n_1$  and  $n_2$  are the asymptotic particle number density. Although this initialization is not a strict 1D kinetic equilibrium [see Alpers, 1969, for one example], any initial transient effects have diminished by the time relatively steady reconnection is occurring. A small magnetic perturbation is used to initiate magnetic reconnection. The reconnection is antiparallel, i.e., there is no guide magnetic field ( $B_z = 0$  at  $t = 0$ ).

[13] In order to test the scaling predictions of equations (1)–(3), we perform simulations of symmetric and asymmetric reconnection with various initial upstream magnetic fields, temperatures, and densities. The parameters for each simulation are shown in Table 1.

[14] Each simulation is evolved until the reconnection reaches a steady state where the reconnection rate  $E$  is relatively constant in time, an example of which is given in Figure 1 for Run BN2b.  $E$  is calculated as the temporal rate of change of magnetic flux between the X line and the O-line. For this particular run, a steady period of reconnection occurs between  $t = 160$  and 220. The oscillations in the reconnection rate during the quasi-steady period allow us to estimate that there is approximately a 10 to 15 percent error in the electric field measurements. During the quasi-steady period of reconnection for Run BN2b, the reconnection exhibits typical ion scale signatures of asymmetric reconnection, as seen in Figure 2, which plots the time averages over  $2 \Omega_{ci0}^{-1}$  of  $n_i$ ,  $J_z$ , and the Hall magnetic field  $B_z$  overlaid with magnetic field lines (lines of constant magnetic flux). The magnetic island preferentially grows into the region with lower magnetic field as has been seen many times before. There is a strong current sheet on the high magnetic field side of the diffusion region, and the quad-

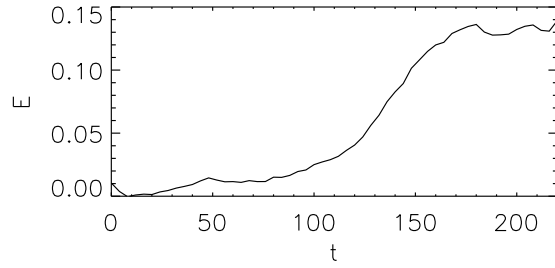


**Figure 1.** Reconnection rate  $E$  versus time  $t$  for Run BN2b. The system exhibits quasi-steady reconnection from  $t = 160$  to 220.

rupolar magnetic field structure is highly distorted [Karimabadi *et al.*, 1999; Mozer *et al.*, 2008a; Tanaka *et al.*, 2008], exhibiting more of a bipolar structure. This distorted  $B_z$  structure does not mean that Hall physics is not playing a role. The existence of a significant  $B_z$  requires currents in the

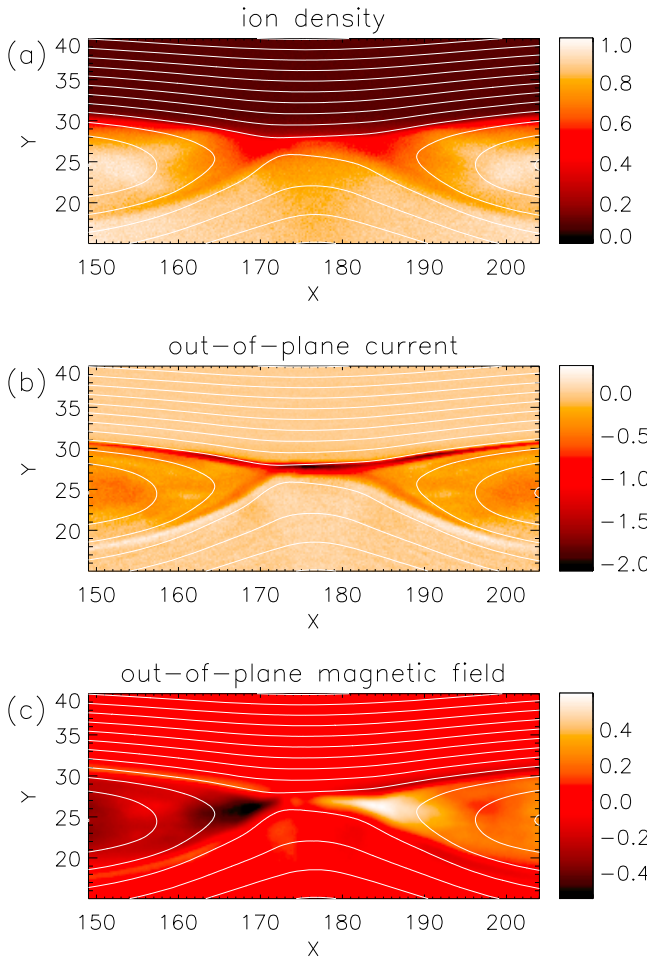


**Figure 2.** Asymmetric reconnection signatures during quasi-steady reconnection of Run BN2b. Contours of constant flux (magnetic field lines) overlaid with (a) ion density  $n_i$ , (b) out-of-plane current  $J_z$ , and (c) out-of-plane magnetic field  $B_z$ . The data for these plots are time averaged from  $t = 180$  to 182.

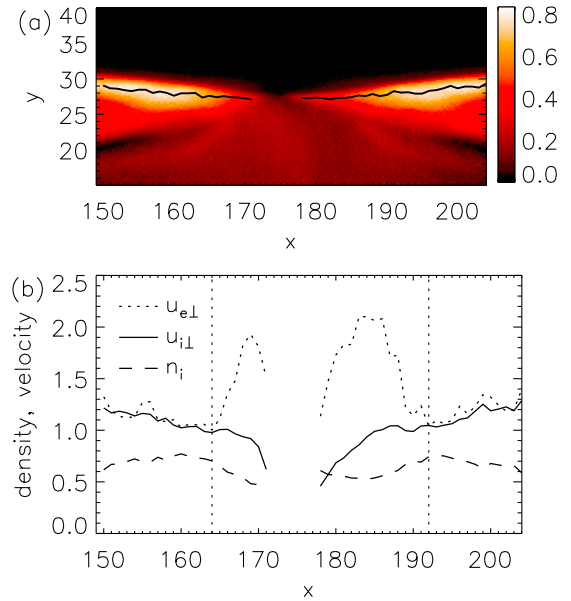


**Figure 3.** Determination of outflow velocities and densities. (a) In-plane ion flux  $n_i u_{i\perp}$ , where the in-plane ion speed  $u_{i\perp} = \sqrt{u_{ix}^2 + u_{iy}^2}$ , showing the path of maximum outflow flux (black line). (b) In-plane ion speed (solid line), in-plane electron speed  $u_{e\perp} = \sqrt{u_{ex}^2 + u_{ey}^2}$ , and downstream density  $n_i$  (dashed line) along the path of maximum ion flux. The data very close to X line, which are not relevant to this study, are omitted because of spurious jumps in the outflow trajectory owing to the very small values of  $n_i u_{i\perp}$ .

$xy$  plane, which implies decoupled electron-ion motion and the importance of Hall physics. The ion density in the downstream diffusion region is clearly a hybrid of  $n_1$  and  $n_2$  [Cassak and Shay, 2007].

[15] Once the system has reached the quasi-steady state, the reconnection rate, outflow speed, and outflow density are measured. In typical symmetric reconnection, downstream properties of the diffusion region (outflow density, outflow speed) can be easily determined by taking a cut along  $x$  at the symmetry line. However, the center of the magnetic islands in asymmetric magnetic reconnection are shifted along the inflow ( $y$ ) direction, and the outflow velocities have a substantial component along  $y$ . In addition, kinetic PIC simulations are inherently noisy, which can make simulation data analysis difficult. To determine the downstream diffusion region properties, we first time average the simulation data over 1 or 2  $\Omega_{ci0}^{-1}$  of the quasi-steady time period. At each  $x$  value, the  $y$  location of the peak in-plane ion flux  $n_i u_{i\perp}$  with  $u_{i\perp} = \sqrt{u_{ix}^2 + u_{iy}^2}$  is determined, as shown in Figure 3a for Run BN2b. The trajectory of these values defines the outflow trajectory away from the diffusion region, which is denoted by the black line in Figure 3a. Plotting  $u_{i\perp}$ ,  $u_{e\perp} = \sqrt{u_{ex}^2 + u_{ey}^2}$  and  $n_i$  along this outflow trajectory allows the determination of downstream diffusion region properties, as shown in Figure 3b. Within a few ion

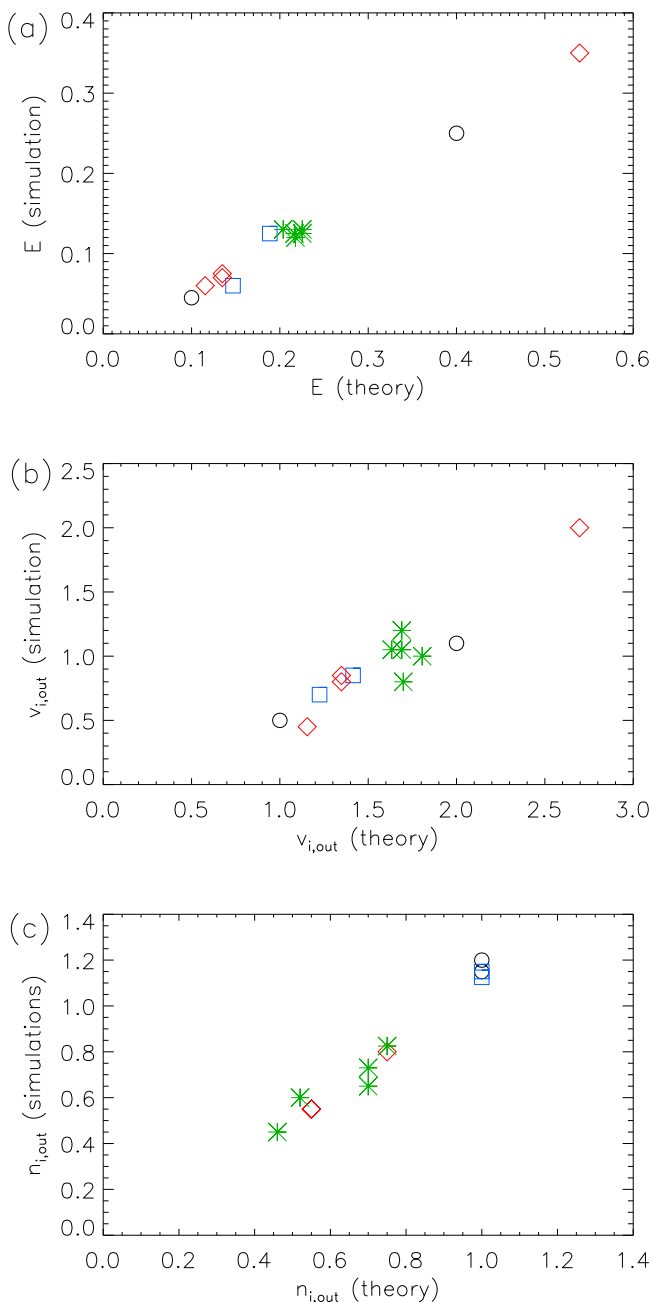


**Figure 4.** Simulation results versus theoretical predictions for (a) reconnection rate  $E$ , (b) outflow speed  $v_{i,out}$ , and (c) outflow density  $n_{i,out}$ . Circles (black) represent symmetric runs. Diamonds (red) represent asymmetric upstream density runs. Squares (blue) represent asymmetric upstream magnetic field runs. Asterisks (green) represent asymmetric upstream density and magnetic field runs.

inertial lengths of the X line the outflow values are not plotted because of spurious jumps of the outflow trajectory owing to the very small values of  $n_i u_{i\perp}$ . As expected near the electron diffusion region, the electrons are decoupled from the ions and thus are super Alfvénic. There is very little ion flow here. The electrons reach a peak velocity which can roughly be thought of as the downstream edge of the elec-

tron diffusion region [Shay *et al.*, 2001]. Their velocity then decreases as they decelerate to join the much slower ions [Shay *et al.*, 1999, 2004]. The location where the electron and ion velocities cross is roughly the location where the ion diffusion region ends, and is denoted by vertical dotted lines in Figure 3b. The ion outflow speed and outflow density are determined by averaging the values at these two locations, as has been done in past two-fluid studies [Shay *et al.*, 2004]. The left-right asymmetry of the diffusion region, as well as scatter in the electron and ion velocities leads to uncertainties in both the location where the electron flow ultimately rejoins the ion flows and the value for  $v_{i,out}$ . We estimate an error of 10 to 15 percent for the ion outflow velocity and the downstream density. The resulting measured reconnection rate, ion outflow speed, and outflow density of each simulation are shown in the last three columns of Table 1.

[16] The measured reconnection rates, outflow speeds, and outflow density from the simulations compare well with the theoretical predictions (equations (1)–(3)), as can be seen in Figure 4. The theoretical values for Figure 4 were determined by using the asymptotic upstream values of the magnetic field and density, a reasonable assumption owing to the initially thin equilibrium current sheets. It was shown in two-fluid studies [Cassak and Shay, 2009] that  $\delta/L$  is approximately 0.1 independent of asymmetries. We employ the analytical technique of making the same assumption here. If the PIC results here agree, we would conclude that the assumption is reasonable. If the data do not fall on a line, we would conclude that kinetic effects beyond the Hall term are altering the structure of the dissipation region. The other reason to assume  $\delta/L \sim 0.1$  is that it is prohibitively difficult to determine  $\delta$  from the simulations because of the noise inherent in kinetic PIC simulations. The absolute magnitude of the theoretical and simulation values for  $E$  and  $v_{out}$  differ by a factor of around 2, though the data falls approximately on a line. The absolute magnitude of the outflow densities show very good agreement between theory and simulations. For all three quantities, the scaling is consistent with the theory [Cassak and Shay, 2007]. The disparity between simulations and theory of around a factor of two is not a concern for the present study. As discussed earlier, scaling analyses can only be expected to be correct up to a factor of order unity. The fact that all three quantities in Figure 3 approximately lie on a line gives evidence that the scaling laws are consistent with simulation results. Clearly, however, there is scatter in the data, which is a result of the uncertainties (of 10 or 15 percent) in determining quantities from the simulations.

#### 4. Discussion and Conclusion

[17] A careful analysis of zero guide field, asymmetric reconnection has been performed using the fully electromagnetic kinetic PIC code P3D. The reconnection rate, ion outflow velocity, and ion outflow density scale as predicted by a Sweet-Parker-like scaling analysis [Cassak and Shay, 2007], assuming the ratio  $\delta/L = 0.1$  within the estimated 10%–15% uncertainty in the simulations. This implies that (1) kinetic physics beyond the Hall term does not fundamentally change the ion scales of the asymmetric diffusion region as understood in the fluid sense [Cassak and Shay,

2007] near the X line, and (2) the assumption that particles on newly reconnected field line fully mix without changing the flux tube volume [Cassak and Shay, 2007] is valid to lowest order, i.e., plasma from just reconnected flux tubes mixes together while preserving the total volume. However, modifications such as including the effects of compressibility and enthalpy flux might improve the accuracy of the predictions [Birn et al., 2010].

[18] As the mixing assumption is valid, we expect the stagnation point locations to match the predictions. However, determining the stagnation point location requires a careful determination of the relatively small inflow velocity which is extremely difficult because of (1) the inherent random noise present in PIC simulations, and (2) the tendency of the X line to propagate along the inflow direction [Jin et al., 2000; Ugai, 2000; Lin, 2001; Cassak and Shay, 2007]. Point (2) requires a shift of reference frames to a frame moving with the X line. This kind of analysis is planned for the future.

[19] This work has limitations which should be addressed in future studies. First, for the dayside magnetosphere, the incoming solar wind often has a significant  $B_y$  component in Geocentric Solar Magnetospheric (GSM) coordinates, which is the equivalent of including a guide magnetic field along  $z$  in this study. This guide field can substantially alter some of the signatures of asymmetric reconnection [Mozer et al., 2008b; Mozer and Pritchett, 2009; Pritchett and Mozer, 2009], although a systematic analysis of its effect on the outflow velocity and reconnection rate has not been performed. In addition, with a guide field the orientation of the X line is uncertain and is the topic of current study [Swisdak and Drake, 2007]. The presence of a pressure gradient across the X line can lead to propagation of the X line due to the diamagnetic drift [Swisdak et al., 2003; Pritchett, 2008]. Second, the analytical scaling study predictions tested here ignore plasma compressibility in the diffusion region, which could lead to a plasma  $\beta$  dependence [Birn et al., 2010]. This  $\beta$  dependence should be considered for future studies, although the effect at typical magnetospheric values may be modest. Finally, the dayside magnetosphere is fundamentally a three-dimensional system, with curvature and three-dimensional stagnation flow effects. Global magnetohydrodynamic simulations of dayside reconnection have found that these 3-D effects can significantly alter the structure of reconnection [Dorelli and Bhattacharjee, 2008, and references therein].

[20] Understanding the physics controlling asymmetric magnetic reconnection will ultimately allow much more realistic predictions for the reconnection signatures in the magnetosphere. These predictions play a critical role in the implementation of satellite missions such as the Magnetospheric Multiscale Mission (MMS).

[21] **Acknowledgments.** This research was supported in part by NASA grants NNX08AM37G and NNX08AO83G, and NSF grants ATM-0645271 and PHY-0902479. Simulations were performed at National Energy Research Scientific Computing Center (NERSC) and National Center for Atmospheric Research Computational and Information System Laboratory (NCAR-CISL).

[22] Philippa Browning thanks David Tsiklauri and another reviewer for their assistance in evaluating this paper.

## References

- Alpers, W. (1969), Steady state charge neutral models of the magnetopause, *Astrophys. Space Sci.*, *5*, 425.
- Birdsall, C., and A. Langdon (1985), *Plasma Physics via Computer Simulation*, McGraw-Hall, New York.
- Birn, J., et al. (2001), GEM magnetic reconnection challenge, *J. Geophys. Res.*, *106*(A3), 3715, doi:10.1029/1999JA900449.
- Birn, J., J. E. Borovsky, and M. Hesse (2008), Properties of asymmetric magnetic reconnection, *Phys. Plasmas*, *15*, 032101.
- Birn, J., J. E. Borovsky, M. Hesse, and K. Schindler (2010), Scaling of asymmetric reconnection in compressible plasmas, *Phys. Plasmas*, *17*, 052108.
- Borovsky, J. E. (2008), The rudiments of a theory of solar wind/magnetosphere coupling derived from first principles, *J. Geophys. Res.*, *113*, A08228, doi:10.1029/2007JA012646.
- Borovsky, J. E., and M. Hesse (2007), The reconnection of magnetic fields between plasmas with different densities: Scaling relations, *Phys. Plasmas*, *14*, 102309.
- Borovsky, J. E., M. Hesse, J. Birn, and M. M. Kuznetsova (2008), What determines the reconnection rate at the dayside magnetosphere?, *J. Geophys. Res.*, *113*, A07210, doi:10.1029/2007JA012645.
- Cassak, P. A., and M. A. Shay (2007), Scaling of asymmetric magnetic reconnection: General theory and collisional simulations, *Phys. Plasmas*, *14*, 102114.
- Cassak, P. A., and M. A. Shay (2008), The scaling of asymmetric hall magnetic reconnection, *Geophys. Res. Lett.*, *35*, L19102, doi:10.1029/2008GL035268.
- Cassak, P. A., and M. A. Shay (2009), Structure of the dissipation region in fluid simulations of asymmetric magnetic reconnection, *Phys. Plasmas*, *16*, 055704.
- Dorelli, J. C., and A. Bhattacharjee (2008), Defining and identifying three-dimensional magnetic reconnection in resistive magnetohydrodynamic simulations of Earth's magnetosphere, *Phys. Plasmas*, *15*, 056504.
- Jin, S. P., J. T. Shen, L. Hao, and X. P. Hu (2000), Numerical study of asymmetric driven reconnection at dayside magnetopause, *Sci. China, Ser. E*, *43*, 129.
- Karimabadi, H., D. Krauss-Vargan, N. Omidi, and H. X. Vu (1999), Magnetic structure of the reconnection layer and core field generation in plasmoids, *J. Geophys. Res.*, *104*(A6), 12,313–12,326, doi:10.1029/1999JA900089.
- Lin, Y. (2001), Global hybrid simulation of the dayside reconnection layer and associated field-aligned currents, *J. Geophys. Res.*, *106*, 25,451–25,466, doi:10.1029/2000JA000184.
- Mozer, F. S., and P. L. Pritchett (2009), Regions associated with electron physics in asymmetric magnetic field reconnection, *Geophys. Res. Lett.*, *36*, L07102, doi:10.1029/2009GL037463.
- Mozer, F. S., V. Angelopoulos, J. Bonnell, K. H. Glassmeier, and J. P. McFadden (2008a), Themis observations of modified hall fields in asymmetric magnetic field reconnection, *Geophys. Res. Lett.*, *35*, L17S04, doi:10.1029/2007GL033033.
- Mozer, F. S., P. L. Pritchett, D. S. J. Bonnell, and M. T. Chang (2008b), Observations and simulations of asymmetric magnetic field reconnection, *J. Geophys. Res.*, *113*, A00C03, doi:10.1029/2008JA013535.
- Nakamura, M., and M. Scholer (2000), Structure of the magnetopause reconnection layer and of flux transfer events: Ion kinetic effects, *J. Geophys. Res.*, *105*(A10), 23,179–23,191, doi:10.1029/2000JA900101.
- Øieroset, M., T. D. Phan, and M. Fujimoto (2004), Wind observations of asymmetric magnetic reconnection in the distant magnetotail, *Geophys. Res. Lett.*, *31*, L12801, doi:10.1029/2004GL019958.
- Phan, T. D., and G. Paschmann (1996), Low-latitude dayside magnetopause and boundary layer for high magnetic shear: 1. Structure and motion, *J. Geophys. Res.*, *101*(A4), 7801, doi:10.1029/95JA03752.
- Pritchett, P. (2008), Collisionless magnetic reconnection in an asymmetric current sheet, *J. Geophys. Res.*, *113*, A06210, doi:10.1029/2007JA012930.
- Pritchett, P. L., and F. S. Mozer (2009), Asymmetric magnetic reconnection in the presence of a guide field, *J. Geophys. Res.*, *114*, A11210, doi:10.1029/2009JA014343.
- Servidio, S., W. H. Matthaeus, M. A. Shay, P. A. Cassak, and P. Dmitruk (2009), Magnetic reconnection in two-dimensional magnetohydrodynamic turbulence, *Phys. Rev. Lett.*, *102*, 115003.
- Shay, M. A., J. F. Drake, B. N. Rogers, and R. E. Denton (1999), The scaling of collisionless, magnetic reconnection for large systems, *Geophys. Res. Lett.*, *26*, 2163, doi:10.1029/1999GL900481.
- Shay, M. A., J. F. Drake, B. N. Rogers, and R. E. Denton (2001), Alfvénic collisionless reconnection and the Hall term, *J. Geophys. Res.*, *106*(A3), 3759, doi:10.1029/1999JA001007.
- Shay, M. A., J. F. Drake, M. Swisdak, and B. N. Rogers (2004), The scaling of embedded collisionless reconnection, *Phys. Plasmas*, *11*(5), 2199.

- Swisdak, M., and J. F. Drake (2007), Orientation of the reconnection x line, *Geophys. Res. Lett.*, *34*, L11106, doi:10.1029/2007GL029815.
- Swisdak, M., J. F. Drake, M. A. Shay, and B. N. Rogers (2003), Diamagnetic suppression of component magnetic reconnection at the magnetopause, *J. Geophys. Res.*, *108*(A5), 1218, doi:10.1029/2002JA009726.
- Tanaka, K. G., et al. (2008), Effects on magnetic reconnection of a density asymmetry across the current sheet, *Ann. Geophys.*, *26*, 2471–2483.
- Ugai, M. (2000), Computer simulations of asymmetric spontaneous fast reconnection, *Phys. Plasma*, *7*, 867.
- Zeiler, A., D. Biskamp, J. F. Drake, B. N. Rogers, M. A. Shay, and M. Scholer (2002), Three-dimensional particle simulations of collisionless magnetic reconnection, *J. Geophys. Res.*, *107*(A9), 1230, doi:10.1029/2001JA000287.
- 
- P. A. Cassak, Department of Physics, West Virginia University, Morgantown, WV 26506, USA.
- C. Bard, K. Malakit, and M. A. Shay, Department of Physics and Astronomy, University of Delaware, 217 Sharp Laboratory, Newark, DE 19716, USA. (kmalakit@udel.edu)